ISSN 0973-2063 (online) 0973-8894 (print)
Bioinformation 22(10): 6535-6542 (2026)
©Biomedical Informatics (2026)

BIOINFORMATION
Discovery at the interface of physical and biological sciences
BIOMEDICAL INFORMATICS
www.bioinformation.net
Volume 22(10)
Research Article

Received October 1, 2026; Revised October 31, 2026; Accepted October 31, 2026, Published October 31, 2026
DOI: 10.6026/973206300226535

SJIF 2026 (Scientific Journal Impact Factor for 2026) = 8.478
2022 Impact Factor (2023 Clarivate Inc. release) is 1.9

Declaration on Publication Ethics:
The author's state that they adhere with COPE guidelines on publishing ethics as described elsewhere at https://publicationethics.org/. The authors also undertake that they are not associated with any other third party (governmental or non-governmental agencies) linking with any form of unethical issues connecting to this publication. The authors also declare that they are not withholding any information that is misleading to the publisher in regard to this article.

Declaration on official E-mail:
The corresponding author declares that lifetime official e-mail from their institution is not available for all authors

License statement:
This is an Open Access article which permits unrestricted use, distribution, and reproduction in any medium, provided the original work is properly credited. This is distributed under the terms of the Creative Commons Attribution License

Comments from readers:
Articles published in BIOINFORMATION are open for relevant post publication comments and criticisms, which will be published immediately linking to the original article without open access charges. Comments should be concise, coherent and critical in less than 1000 words.

Disclaimer:
Bioinformation provides a platform for scholarly communication of data and information to create knowledge in the Biological/ Biomedical domain after adequate peer/editorial reviews and editing entertaining revisions where required. The views and opinions expressed are those of the author(s) and do not reflect the views or opinions of Bioinformation and (or) its publisher Biomedical Informatics. Biomedical Informatics remains neutral and allows authors to specify their address and affiliation details including territory where required.

Edited by P Kangueane
Citation: Kumari *et al.* Bioinformation 22(10): 6535-6542 (2026)

In silico analysis of and rogenetic alopecia-relevant compounds targeting steroid 5α-reductase

Kriti Kumari[1,*], S.M. Shayez Karim[2] & R.S. Rathore[1]

[1]Department of Bioinformatics, Central University of South Bihar, Gaya, Bihar, India; [2] Department of Biotechnology, IILM University, Greater Noida, Uttar Pradesh, India; *Corresponding author

Affiliation URL:
https://cusb.ac.in/
https://iilm.edu/

Author contact:
Kriti Kumari - E-mail: kriti@cusb.ac.in
S.M. Shayez Karim - E-mail: shayez.karim@iilm.edu
R.S. Rathore - E-mail: rsrathore@cusb.ac.in

ISSN 0973-2063 (online) 0973-8894 (print)
Bioinformation 22(10): 6535-6542 (2026)
©Biomedical Informatics (2026)

Abstract:
SRD5A converts testosterone to 5α-dihydrotestosterone, the key androgen driving androgenetic alopecia (AGA) and the target of finasteride/dutasteride. Docking and MM-GBSA rescoring of nine chemically diverse AGA-relevant compounds identified bimatoprost and EGCG as the top docking hits, while MM-GBSA rescoring instead favoured latanoprost (ΔG_bind = −58.1 kcal/mol) and dutasteride (−48.1 kcal/mol). EGCG, bimatoprost and taxifolin formed a closely-tied second MM-GBSA tier (≈−42 to −43 kcal/mol), with the two scoring stages agreeing only loosely across this chemically heterogeneous panel (Pearson r = 0.58). A 100 ns MD simulation showed the PbSRD5A–EGCG complex reaching stable equilibrium after ~30 ns, with sustained NADPH-proximal contacts, while a parallel finasteride simulation showed comparable protein stability but a higher, more variable ligand RMSD. These findings suggest several structurally diverse AGA therapeutics may exert contributory effects via direct SRD5A engagement.

Keywords: Androgenetic alopecia, Steroid 5α-reductase, Molecular docking, MM-GBSA, Molecular dynamics simulation, PbSRD5A, EGCG, Finasteride

Background:
Androgenetic alopecia (AGA) is characterized by hair follicle miniaturization driven by androgen signaling **[1, 2]**. Steroid 5α-reductases (SRD5A1 and SRD5A2) catalyze the NADPH-dependent reduction of testosterone to 5α-dihydrotestosterone (DHT), which possesses significantly higher affinity for the androgen receptor **[3]**. While pharmacological research has focused on 4-azasteroids like finasteride, the potential for non-steroidal marketed AGA ligands to directly inhibit SRD5A remains poorly characterized **[4]**. Recent computational studies have identified candidate non-classical SRD5A-targeting compounds, including phytosterols such as beta-sitosterol **[5]**, plant-derived diterpenoids combining 5α-reductase-inhibitory and anti-inflammatory activity **[6]** and DrugBank compounds repositioned against SRD5A2 **[7]**, underscoring the value of structure-based screening for AGA-relevant SRD5A ligands. This study utilizes the crystal structure of PbSRD5A, a bacterial homolog from a Proteobacterium sharing approximately 60% and 51% sequence similarity with human SRD5A1 and SRD5A2, respectively, was solved at 2.0 Å resolution in complex with the reduced cofactor NADPH (PDB 7C83) to evaluate whether chemically diverse AGA ligands can occupy the cofactor-binding cavity, providing a structural basis for potential secondary mechanisms of action **[8]**. The structure revealed a seven-transmembrane-helix monomeric fold in which helices TM1–TM4 enclose a hydrophobic substrate-binding cavity and TM5–TM7 coordinate NADPH through an extensive hydrogen-bond network involving Asn159, Asp163 and Arg170 (TM5), Asn192, Tyr193 and Glu196 (TM6) and Thr219, Asn222, Arg226 and His230 (TM7), together with Tyr32 and Arg34 on intracellular loop 1 and Tyr177 on loop 3 **[8, 9]**. This residue set defines the chemical environment available for cofactor-proximal ligand recognition. Therefore, it is of interest to investigate whether chemically diverse AGA ligands can engage this cavity and provide a structural basis for potential secondary modulation of SRD5A.

Materials and Methods:
Protein preparation:
The crystal structure of PbSRD5A (PDB: 7C83, the available highest 2.0 Å resolution structure) used as the structural template. A receptor grid was centered on the NADPH-proximal cavity, defined by residues reported to coordinate the cofactor (TM5–TM7 and intracellular loops 1 and 3). Protein preparation and protonation were performed using the Protein Preparation Wizard (Schrödinger Suite 2022-4) **[10]**. Ligands were prepared via LigPrep to ensure accurate ionization states. Molecular docking was executed using Glide SP, followed by binding free energy estimation via Prime MM-GBSA **[11]** under the VSGB 2.0 solvation model **[12]**. A 100 ns molecular dynamics (MD) simulation of the EGCG complex was conducted using the Desmond engine (NPT ensemble, 300 K) to validate pose stability, alongside a parallel 100 ns simulation of the finasteride complex under identical conditions as a reference control.

Ligand set:
The 25 marketed drugs for alopecia were used with diverse chemical classes. The ligand group shown here in **Table 1** is selected based on their binding affinity to target 7C83. Ligands were fetched from PubChem Compound ID (CID) **[13]** and prepared with correct protonation/ionization states (*e.g.*, carboxylate and ammonium forms) before docking by Ligprep.

Docking and MM-GBSA rescoring:
The docking of all ligands was done into the receptor grid (7C83_grid.zip) using Glide SP **[14, 15]** each ligand completed docking successfully (docking status "Done" for all), returning a Glide Docking Score, GlideScore (gscore) and the standard Glide energy-term decomposition (lipophilic, hydrogen-bond (H-bond), van der Waals (Evdw), Coulombic (Ecoul), rotatable-bond penalty (Erotb), site, model [Emodel] and internal strain (Einternal) energies) for the top-ranked pose of each compound. In the second (rescoring) stage, the top Glide pose for each ligand was rescored using Prime MM-GBSA (Molecular Mechanics – Generalized Born Surface Area), which decomposes the predicted binding free energy (ΔG_bind) into Coulombic (electrostatic), H-bond, lipophilic, van der Waals (vdW), π–π packing, self-contact and generalized-Born/surface-area solvation (Solv_GB) terms. Ligand strain energy and the normalized ligand efficiency (ΔG_bind scaled by a measure of ligand size) were also computed for each pose. Two-dimensional protein–ligand interaction diagrams were generated for each docked complex to visualize hydrogen bonds, salt bridges and hydrophobic contacts with active-site residues within approximately 4–5 Å of the ligand. Docking with another structure of SRD5A (PDB Id: 7BW1) was also carried out and

results are given in Supplementary Material. As a further validation, the docked finasteride pose (PbSRD5A, 7C83) and the crystallographic finasteride pose in 7BW1 (bound as its covalent NADP–dihydrofinasteride adduct) were compared after structural superposition of the two receptors (2.11 Å Cα RMSD over 243 corresponding residues); the docked ligand retained a similar internal conformation (1.35 Å ligand RMSD) but adopted a divergent binding-site pose (5.73 Å ligand RMSD) relative to the crystal structure, consistent with the moderate sequence divergence between the two SRD5A homologs.

Results:

The predicted binding free energies spanned a range from −58.1 kcal/mol (latanoprost) to −19.8 kcal/mol (beta-sitosterol), an approximately 2.9-fold spread across the series **(Table 3)**. Latanoprost and dutasteride formed a clear high-affinity tier (ΔG_bind ≤ −48 kcal/mol), both driven by large, favourable lipophilic and van der Waals terms consistent with their extended aliphatic/steroidal scaffolds. A second, closely-grouped tier (taxifolin, EGCG and bimatoprost; −42 to −43 kcal/mol, essentially tied) combined moderate lipophilic burial with, for EGCG specifically, a large but largely self-cancelling polar (Coulomb/Solv_GB) contribution from its polyphenolic hydroxyl network. Caffeine, Ac-SDKP, melatonin and beta-sitosterol formed the weakest tier (−20 to −35 kcal/mol). Binding free energy and ligand efficiency told different stories: caffeine, despite the second-lowest absolute ΔG_bind, achieved the best ligand efficiency of any compound tested (−2.48), reflecting its small molecular size relative to the binding energy recovered, while beta-sitosterol, the bulkiest ligand in the set had the poorest efficiency (−0.66) despite a large lipophilic term, indicating its binding energy is spread over a large, less efficiently packed steroid scaffold. Ac-SDKP, a flexible tetrapeptide, showed by far the largest raw Coulombic and desolvation terms in the panel (Coulomb −126.5 / Solv_GB +155.5 kcal/mol, roughly three times any other ligand's), yet converted comparatively little of that raw electrostatic interaction into net efficient binding (ligand efficiency −0.95), reflecting the cost of burying its charged Asp/Lys side chains and free termini. Initial Glide SP docking **(Table 2)** ranked the series bimatoprost > EGCG > latanoprost > dutasteride > taxifolin > beta-sitosterol > melatonin > caffeine > Ac-SDKP. Subsequent Prime MM-GBSA rescoring **(Table 3)** reordered this substantially: latanoprost and dutasteride, only third and fourth by docking score, became the two most favourable binders by ΔG_bind, while beta-sitosterol, sixth by docking, fell to last by MM-GBSA once desolvation costs were included. Docking score and ΔG_bind correlated only weakly across the series overall (Pearson r = 0.58, p = 0.099; **Figure 1**), a marked contrast with a more chemically homogeneous ligand panel, where the two stages tracked closely GlideScore favours pose complementarity and can be dominated by a single strong contact, whereas Prime MM-GBSA's Generalized Born desolvation term can substantially discount or reward scaffolds unevenly depending on their polarity, so the two stages are best interpreted together rather than singly for a chemically diverse set like this one. Latanoprost illustrates this most starkly, a mid-pack Glide score (−7.76, fifth-best) paired with by far the best MM-GBSA ΔG_bind, driven by large favourable lipophilic (−30.5 kcal/mol) and van der Waals (−36.0 kcal/mol) terms with comparatively modest desolvation cost (Solv_GB +20.5 kcal/mol) the most favourable such balance in the panel. EGCG's affinity, by contrast, is carried by a different mechanism: a large favourable Coulombic term (−44.9 kcal/mol) from its polyphenolic hydroxyl network, almost entirely offset by an equally large desolvation penalty (+43.1 kcal/mol), so its net affinity ends up similar in magnitude to bimatoprost's purely lipophilic burial despite the very different underlying chemistry. Dutasteride and finasteride, the two 4-azasteroid 5α-reductase inhibitors in this comparison, show closely similar energy profiles (dutasteride ΔG_bind −48.1 kcal/mol vs finasteride's −43.4 kcal/mol; both dominated by van der Waals packing with minimal polar contribution), consistent with their shared steroidal scaffold and mechanism. The dominant MM-GBSA energy contributions, binding modes and residue-level interactions identified for each compound through docking-pose and interaction-diagram analyses are summarized in **Table 4**. EGCG's galloyl ester and pyrogallol/catechol rings form an extensive H-bond network with Asn159, Tyr193, Asp163, Glu196 and Val100/Met98/Arg99, while the flavan chroman ring system and second trihydroxyphenyl group pack against Leu166/Arg167/Arg170/Tyr177/Leu169, with Trp50, Tyr32/Gly33, His230 and Thr45/Ala102/Gly101 completing the boundary **(Figure 2)**. The combination of numerous hydroxyl-mediated H-bonds with aromatic/lipophilic burial across a large, polyphenolic surface area is consistent with EGCG's strong, near-top-tier ΔG_bind and among the best ligand efficiencies in the series. This ligand follows the experimental literature as EGCG has been shown in cell-free assays to directly inhibit human 5α-reductase, with selectivity toward the type-1 isoform and separately to promote proliferation-associated markers in cultured human hair follicles. The residues of the docked pose contain Asp163, Tyr193, Glu196 and Asn159, which are the same ones the crystal structure assigns to NADPH nicotinamide/ribose coordination, giving a specific structural candidate for where that enzymatic inhibition might physically occur. The stability of the docked EGCG–protein complex under physiologically relevant conditions was assessed using a 100 ns molecular dynamics (MD) simulation (Figure 4). Protein Cα RMSD increased during the initial ~30 ns, reflecting an equilibration phase and subsequently stabilized within an approximately 3.0–4.5 Å range for the remainder of the trajectory. This pattern suggests that the overall structural integrity of the seven-transmembrane helical bundle was maintained throughout the simulation. The ligand RMSD followed a similar trend, plateauing at approximately 3–4.5 Å after the same initial period, with a single transient excursion to ~6.6 Å near 70 ns that relaxed back to baseline within a few nanoseconds - a comparatively small, short-lived departure from the initial docking geometry rather than a sustained relocation. RMSF analysis highlighted the highest mobility in the 165–180 loop (loop 3), consistent with this region's role in the EGCG H-

bond/van der Waals network described above, along with smaller mobility peaks around residues 90–100 and 30–35. The interaction analysis revealed sustained engagement of EGCG with several NADPH-proximal residues, including Arg90, Met98, Tyr193 and Glu196, throughout the trajectory. A comparatively lower-persistence water-bridge interaction was also observed at Arg226 **(Figure 3)**. The consistent contact pattern and ligand RMSD, together with the absence of an apparent transition to a distinct surface site, suggest that EGCG predominantly retained its cofactor-proximal binding mode during the 100 ns simulation. A parallel 100 ns finasteride-control simulation in **Figure 4**, reached a comparable protein RMSD plateau (~3.0–3.5 Å) but showed a consistently higher, more variable ligand RMSD (~4.3 Å vs EGCG's ~3.2 Å over the 10–80 ns window), suggesting greater positional drift of finasteride within the cavity relative to EGCG . Bimatoprost's cyclopentane diol core and flanking unsaturated chains build a long hydrophobic channel lined by Phe94, Trp50, Tyr32/Gly33/Arg34, Asn159, Tyr193/Asn192, Glu196, Leu166/Arg167/Leu169/Arg170 and Tyr177/Glu178/Pro180, with its terminal N-ethylamide group positioned near Arg176/Tyr177 **(Figure 2)**. The large favourable lipophilic (−32.2 kcal/mol) and van der Waals (−47.7 kcal/mol) terms dominate its net binding energy, consistent with a pose that maximizes burial of hydrophobic surfaces. Bimatoprost acts through prostamide receptors to shift follicles from telogen into anagen and has been shown to outperform minoxidil in some animal AGA models. Ac-SDKP, the endogenous regulatory tetrapeptide, engages the same cavity through a distinct, largely electrostatic mechanism: salt bridges and hydrogen bonds to Glu54 and Asn222 anchor its charged Lys side chain and C-terminal carboxylate, with Trp50 and Leu112/Ala113 lining the remainder of the pocket (**Figure 2**, panel I), though the unusually large cost of desolvating those charged groups (Solv_GB +155.5 kcal/mol) limits its net binding efficiency relative to the panel's more lipophilic ligands, despite its raw Coulombic term being the largest in the series. Latanoprost and bimatoprost share H-bond anchors at Ser21 and Asn222, consistent with their common prostaglandin scaffold; dutasteride, caffeine and finasteride each engage the pocket with no hydrogen-bond anchor at all, matching their near-zero Glide H-bond terms **(Table 2)** and instead rely on purely hydrophobic or π-stacking contact (Phe17/Phe116/Phe176/Phe218, Ala113, Leu112).

Table 1: Identity and AGA-focused pharmacological rationale for the nine ligands with good binding against PbSRD5A (PDB 7C83)

PubChem CID	Compound	Chemical class	AGA / anti-androgen relevance
5311027	Bimatoprost	Synthetic prostamide (PGF2α analogue)	Prostaglandin analogue clinically associated with enhanced hair/eyelash growth (marketed as Latisse); reviewed for scalp AGA use **[15, 16]**.
65064	(−)-Epigallocatechin-3-gallate (EGCG)	Flavan-3-ol gallate ester (green-tea catechin)	Polyphenols are reported to inhibit human 5α-reductase directly and to stimulate hair follicle growth markers **[17, 18]**.
5311221	Latanoprost	Synthetic prostaglandin F2α analogue (isopropyl ester)	Structurally related to bimatoprost; a randomized placebo-controlled pilot trial reported increased scalp hair growth with topical latanoprost 0.1% in androgenetic alopecia **[19]**.
6918296	Dutasteride	4-azasteroid, dual Type 1/Type 2 5α-reductase inhibitor	Randomized trials report superior dihydrotestosterone suppression and hair-growth efficacy versus finasteride in male pattern hair loss **[20]**.
439533	Taxifolin	Dihydroflavonol (flavonoid)	Structurally related to EGCG's catechin scaffold; shown to suppress rat and human testicular androgen-biosynthetic enzyme activity *in vitro* **[21]**.
222284	Beta-sitosterol	Phytosterol	Principal sterol component of saw palmetto extract; a randomized placebo-controlled trial of botanically-derived 5α-reductase inhibitors reported improved androgenetic alopecia outcomes **[22]**.
896	Melatonin	Indoleamine hormone (tryptophan derivative)	Topical antioxidant reported to increase anagen hair rate in a pilot randomized controlled trial in women with androgenetic or diffuse alopecia **[23]**.
2519	Caffeine	Methylxanthine alkaloid	Common ingredient in anti-hair-loss topical formulations; shown to counteract testosterone-induced suppression of human hair follicle proliferation *ex vivo* **[24]**.
4409396	N-Acetyl-Ser-Asp-Lys-Pro (Ac-SDKP)	Endogenous tetrapeptide	Natural regulatory peptide shown to stimulate elongation of cultured human hair follicles and epidermal renewal **[25]**; used in cosmetic/dermatologic scalp formulations.

Table 2: Glide docking-stage scores and energy terms for the top pose of each of the nine top-ranked test ligands against the receptor grid (7C83_grid.zip) and finasteride (57363), docked under identical conditions and appended below as the reference SRD5A-targeting control

Compound	ΔG_bind (kcal/mol)	Coulomb	H bond	Lipophilc	vdW	Solv_GB	Ligand efficiency
Bimatoprost (5311027)	-8.27	-8.27	-4.26	-0.67	-44.37	-10.40	-74.57
EGCG (65064)	-8.25	-8.34	-3.97	-0.09	-9.84	-23.52	-33.01
Latanoprost (5311221)	-7.76	-7.76	-5.03	-0.86	-34.32	-5.74	-53.05
Dutasteride (6918296)	-7.60	-7.60	-3.98	0.00	-39.59	-0.42	-53.82
Taxifolin (439533)	-7.11	-7.15	-3.26	-0.14	-36.97	-2.60	-56.36
Beta-sitosterol (222284)	-7.08	-7.08	-4.86	-0.32	-27.62	-1.72	-28.68
Melatonin (896)	-6.87	-6.87	-3.00	-0.43	-35.02	-5.10	-51.22
Caffeine (2519)	-6.80	-6.80	-1.33	0.00	-26.93	-1.59	-40.31
Ac-SDKP (4409396)	-6.70	-6.70	-3.16	-0.16	-33.97	-8.97	-53.18
Finasteride (57363)	-6.14	-6.14	-3.07	0.00	-38.00	-0.15	-48.86

The docked finasteride pose in PbSRD5A (7C83) was compared with the crystallographic finasteride pose in human SRD5A2 (7BW1, present as its covalent NADP–dihydrofinasteride adduct) after structural superposition of the two receptors (2.11 Å Cα RMSD over 243 corresponding residues). Ligand RMSD relative to the crystal structure: 5.73 Å in the shared, aligned receptor frame; 1.35 Å after independently re-superposing the ligand alone (conformation only). See Supplementary Material for full methodology.

Table 3: Prime MM-GBSA binding free energy and energy-component decomposition for the nine prioritized test ligands, ranked from most to least favourable ΔG_bind, plus finasteride (57363), docked and rescored under identical conditions and appended below as the reference SRD5A-targeting control also used in the MD comparison **(Figure 4)**. Ligand efficiency is the Prime-normalized ΔG_bind per unit of ligand size (dimensionless within this series; more negative indicates better efficiency)

Compound	ΔG_bind (kcal/mol)	Coulomb	H-bond	Lipophilic	vdW	Solv_GB	Ligand efficiency	Combined Rank
Latanoprost (5311221)	-58.13	-14.27	-1.58	-30.50	-35.99	20.52	-1.88	3
Dutasteride (6918296)	-48.11	-5.79	-0.01	-24.19	-37.96	18.68	-1.30	4
Taxifolin (439533)	-42.94	-9.11	-0.90	-14.66	-37.57	19.81	-1.95	5
EGCG (65064)	-42.23	-44.93	-4.45	-27.50	-28.36	43.12	-1.28	2
Bimatoprost (5311027)	-42.19	-10.36	-2.59	-32.20	-47.66	42.41	-1.41	1
Caffeine (2519)	-34.72	-12.08	-0.03	-7.56	-31.13	19.52	-2.48	8
Ac-SDKP (4409396)	-32.32	-126.52	-2.11	-16.96	-46.07	155.52	-0.95	9
Melatonin (896)	-27.59	-9.35	-1.50	-13.68	-40.81	34.35	-1.62	7
Beta-sitosterol (222284)	-19.79	-6.78	-0.79	-36.81	-22.69	34.04	-0.66	6
Finasteride (57363)	-43.38	-4.68	-0.01	-23.15	-37.87	21.54	-1.61	Control

Table 4: Ligands grouped by dominant MM-GBSA energy signature ("binding strategy") at the shared PbSRD5A cofactor-proximal cavity, alongside each compound's independently established, non-SRD5A pharmacological route to a hair-growth effect

Compound	Dominant MM-GBSA term(s)	Structural binding strategy	Independent, non-SRD5A pharmacological route (ref.)
Bimatoprost	Lipophilic −32.2 / vdW −47.7 (both large and favourable)	Lipophilic surface-burial: long aliphatic–aromatic chain maximizing hydrophobic channel occupancy against Phe17/Phe176/Phe218 and Tyr87, anchored by H-bonds to Ser21, Glu54 and Asn222 (Figure 2)	Prostamide (FP) receptor agonism; anagen-phase prolongation **[15, 16]**
Latanoprost	Lipophilic −30.5 / vdW −36.0 (both large and favourable)	Lipophilic surface-burial: isopropyl-ester tail and cyclopentane ring occupy the same hydrophobic channel as bimatoprost, consistent with their shared prostaglandin scaffold, anchored by H-bonds to Ser21 and Asn222 (Figure 2)	Prostamide/FP receptor agonism; topical trial reported increased scalp hair growth **[19]**
Dutasteride	vdW −38.0 / Lipophilic −24.2 (large, favourable; negligible polar contribution)	Steroidal lipophilic burial: 4-aza-3-oxo-steroid core and bis(trifluoromethyl)phenyl group packed against Phe17/Phe176/Phe218 and Ala113/Ala118, the same reductive substrate class SRD5A evolved to process, with no hydrogen-bond anchor observed (Figure 2), consistent with its near-zero Glide H-bond term	Dual Type 1/Type 2 5α-reductase inhibition; superior DHT suppression vs finasteride in RCTs **[20]**
EGCG	Coulomb −44.9 / Solv_GB +43.1 (large, near-cancelling); Lipophilic −27.5 / vdW −28.4	Multipoint H-bonding plus extensive aromatic/hydroxyl contact across a large polyphenolic surface, with H-bonds to Glu64, Tyr32 and Asn222 (Figure 2)	Direct cell-free inhibition of human 5α-reductase; antioxidant and enzyme-modulatory activity **[17, 18]**
Taxifolin	vdW −37.6 / Lipophilic −14.7 (favourable; smaller Coulomb −9.1 than EGCG)	Smaller dihydroflavonol scaffold combining moderate H-bonding at Thr109 with hydrophobic packing of its two aromatic rings against Asn117/Phe176/Leu112 (Figure 2)	Suppresses testicular androgen-biosynthetic enzyme activity *in vitro* **[21]**
Beta-sitosterol	Lipophilic −36.8 (largest lipophilic term in the panel) / Solv_GB +34.0	Lipophilic surface-burial: rigid tetracyclic sterol ring system and branched alkyl tail maximize hydrophobic contact against Phe176/Phe215/Phe218 and Leu112, minimal polar anchoring beyond a single H-bond at Asn117 (Figure 2)	Major sterol of saw palmetto extract; botanical 5α-reductase inhibitor with RCT-reported AGA benefit **[20]**
Melatonin	vdW −40.8 / Solv_GB +34.4 (moderate Coulomb −9.4)	Compact indoleamine packing its methoxy-indole ring and acetamide group into the hydrophobic channel against Trp50, Ala113 and Tyr32, with a modest polar anchor at Glu54 (Figure 2)	Topical antioxidant reported to increase anagen hair rate in a pilot RCT **[23]**
Caffeine	vdW −31.1 / Coulomb −12.1 (smallest molecule in the panel)	Small, rigid xanthine ring stacking within the pocket against Phe116/Ala113/Leu112; modest absolute binding energy but the most efficient packing per atom in the series, with no hydrogen-bond anchor observed (Figure 2)	Counteracts testosterone-induced suppression of hair follicle proliferation *ex vivo* **[24]**
Ac-SDKP	Coulomb −126.5 /	Electrostatic-anchor, desolvation-limited: discrete salt bridges/H-bonds to Glu54	Endogenous regulatory

ISSN 0973-2063 (online) 0973-8894 (print)
Bioinformation 22(10): 6535-6542 (2026)
©Biomedical Informatics (2026)

Solv_GB (large, near-cancelling)	+155.5	(NζH3+ terminus) and Asn222 (C-terminal carboxylate) anchor its charged side chains, with Trp50 and Leu112/Ala113 lining the remainder of the pocket (Figure 2), capped by the cost of burying those polar groups	tetrapeptide; direct stimulation of hair-follicle elongation and epidermal renewal markers **[25]**

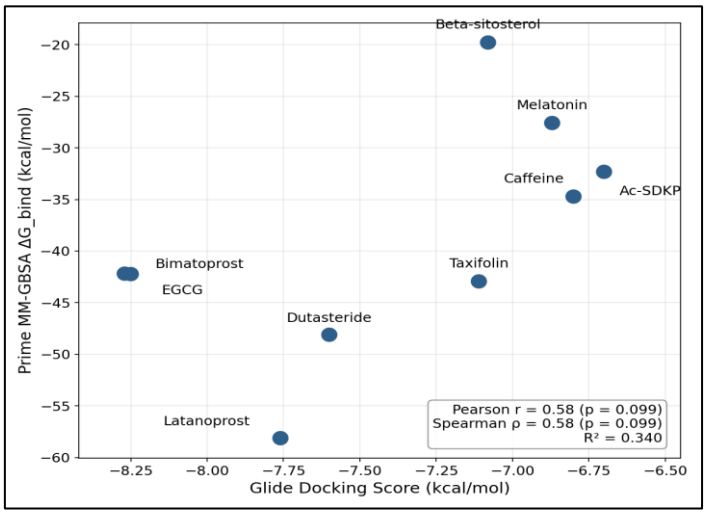


Figure 1: Correlation between Glide Docking Score (Table 2) and Prime MM-GBSA ΔG_bind (Table 3) for all nine docked test ligands. All nine ligands (blue dots) are shown. Pearson r = 0.58 (p = 0.099) and Spearman ρ = 0.58 (p = 0.099) (linear R^2 = 0.340), indicating that for this chemically diverse panel the two scoring stages agree loosely due to Ac-SDKP, Bimatoprost and EGCG, which acts as outliers due to high desolvation cost (not considered during docking)

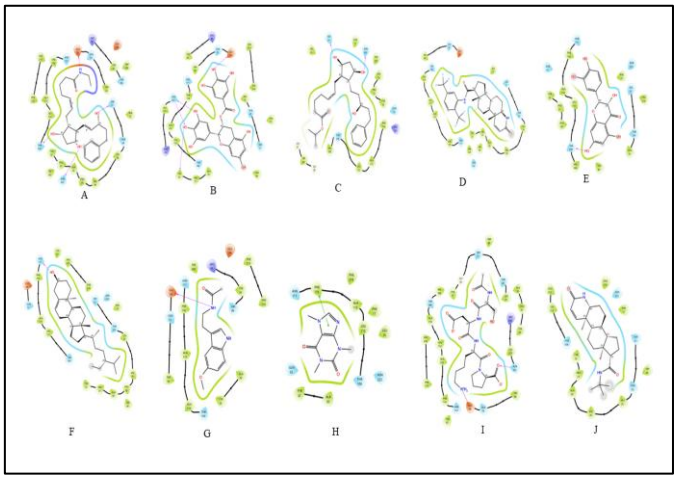


Figure 2: Two-dimensional protein–ligand interaction diagrams for all nine test ligands and the finasteride control within the PbSRD5A (PDB: 7C83) active site. (A) Bimatoprost (CID 5311027), (B) EGCG (CID 65064), (C) Latanoprost (CID 5311221), (D) Dutasteride (CID 6918296), (E) Taxifolin (CID 439533), (F) Beta-sitosterol (CID 222284), (G) Melatonin (CID 896), (H) Caffeine **(CID** 2519), (I) Ac-SDKP (CID 4409396) and (J) Finasteride (CID 57363), the reference SRD5A-targeting control. Coloured residue markers follow standard convention (green = hydrophobic, cyan = polar, purple = basic, orange = acidic); magenta dashed arrows mark hydrogen bonds

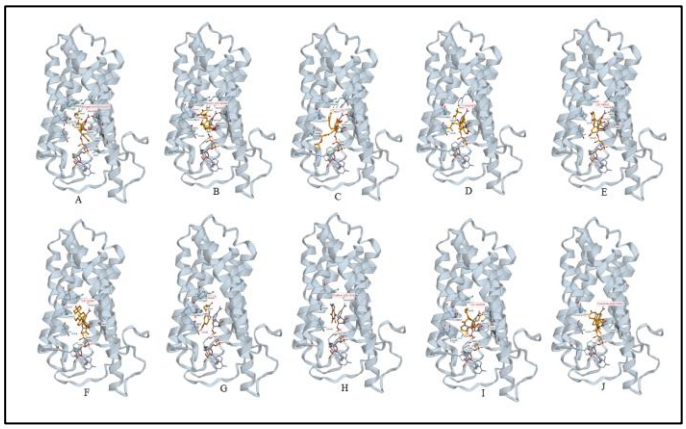


Figure 3: Three-dimensional binding modes of all nine test ligands and the finasteride control within the PbSRD5A (PDB: 7C83) active site. (A) Bimatoprost (CID 5311027), (B) EGCG (CID 65064), (C) Latanoprost (CID 5311221), (D) Dutasteride (CID 6918296), (E) Taxifolin (CID 439533), (F) Beta-sitosterol (CID 222284), (G) Melatonin (CID 896), (H) Caffeine (CID 2519), (I) Ac-SDKP (CID 4409396) and (J) Finasteride (CID 57363), the reference SRD5A-targeting control. Docked poses highlight convergence of these nine structurally diverse scaffolds onto the shared cofactor-proximal cavity

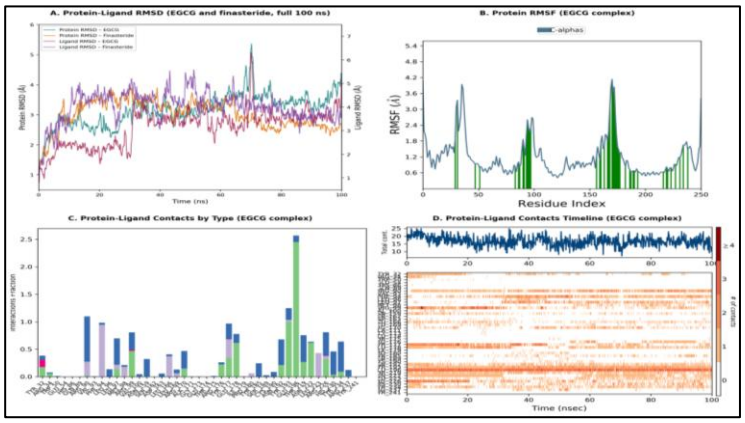


Figure 4: A 100 ns molecular dynamics summary of the PbSRD5A (7C83)–EGCG complex, with a parallel PbSRD5A–finasteride simulation overlaid for comparison. (A) Protein Cα RMSD (left axis) and ligand 'fit-on-protein' RMSD (right axis) versus simulation time for both complexes (EGCG protein RMSD- teal, finasteride protein RMSD- orange, EGCG ligand RMSD- crimson, finasteride ligand RMSD- purple). (B) Protein RMSF by residue index for the PbSRD5A backbone in the EGCG complex; green bars mark residues in ligand contact. (C) Protein–ligand contacts summed over the trajectory and broken down by interaction type (H-bonds, hydrophobic, ionic, water bridges) for the EGCG complex. (D) Per-residue contact timeline for the EGCG complex, with the total contact count shown above

Discussion:

The observed binding energetics reveal five structurally coherent binding strategies across the panel **(Table 4)**. The two prostaglandin F2α analogues, bimatoprost and latanoprost, both derive their affinity from lipophilic surface-burial of an extended aliphatic–aromatic chain within the hydrophobic channel, with only a single polar anchor near the amide/ester terminus consistent with their shared FP-receptor pharmacology and their close energetic similarity in **Table 3**. Dutasteride, the only other steroidal 5α-reductase inhibitor in the set besides the finasteride control, likewise binds through steroidal lipophilic burial with minimal polar contribution and its energy profile closely resembles finasteride's **(Table 3)** unsurprising given the two shares both chemical scaffold and enzymatic mechanism. The two flavonoids, EGCG and taxifolin, form a third group: EGCG's larger catechin-gallate scaffold builds an extensive, largely polar network (Coulomb −44.9 which however is cancelled by large desovlation cost, Solv_GB +43.1 kcal/mol) and moderate lipophilic packing, while taxifolin's smaller dihydroflavonol core relies more on van der Waals contact with a comparatively modest Coulombic contribution. A fourth group comprises beta-sitosterol (consistent with its prior identification as an SRD5A1 ligand by independent computational screening **[5]**), melatonin and caffeine, three smaller, chemically distinct ligands that each bind through comparatively compact, single-mechanism packing (lipophilic for the sterol, van der Waals for the indoleamine and the xanthine), with caffeine standing out for the best ligand efficiency in the series despite its modest absolute affinity. A fifth, mechanistically distinct group is represented by Ac-SDKP, the only peptide in the panel: its binding is dominated by an unusually large Coulombic term (−126.5 kcal/mol) from salt bridges and hydrogen bonds formed by its charged Asp/Lys side chains and free termini, almost entirely offset by an equally large desolvation penalty (Solv_GB +155.5 kcal/mol) the most extreme electrostatic-anchor/desolvation trade-off in the series, consistent with the general difficulty small polar or charged peptides face in achieving efficient burial within a predominantly hydrophobic cavity. A 100 ns MD simulation of the PbSRD5A–EGCG complex **(Figure 4)** supports EGCG's docking pose: after an initial ~30 ns adjustment period, both the protein Cα backbone and the ligand settle into a broadly stable regime (protein RMSD ~3–4 Å; ligand RMSD ~3–4 Å), interrupted only by a single transient excursion near 70 ns that quickly relaxes back to baseline. RMSF peaks localize to the same NADPH-proximal loop regions (around residues 90–100 and 170–196) that dominate the per-residue contact profile, with several residues in this range (e.g., Arg90, Met98, Tyr193, Glu196) showing sustained, near-continuous contact throughout the trajectory rather than a transient interaction. A parallel 100 ns PbSRD5A–finasteride simulation, overlaid in Figure 4A, reaches a comparable protein Cα RMSD plateau to the EGCG complex (~3.0–3.5 Å for both systems after the initial adjustment period), indicating similar global backbone stability regardless of which ligand is bound. The two ligands' RMSD profiles diverge more: over the 10–80 ns window, finasteride's ligand RMSD runs consistently higher than EGCG's (~4.3 Å vs ~3.2 Å on average), suggesting greater positional drift of finasteride within the cavity, although the two converge over the final 20 ns of the run (~3.6–3.7 Å for both). Collectively, these results suggest that several structurally distinct AGA-relevant compounds **[26-29]** may provide additive clinical benefits by acting as "cofactor decoys" or surface-level inhibitors of SRD5A.

Conclusion:

This study provides a structural basis for the potential secondary pharmacology of marketed and nutraceutical AGA-relevant compounds through SRD5A cofactor-cavity engagement, with latanoprost, dutasteride and EGCG emerging as the most favourable predicted binders. A 100 ns MD simulation confirmed a stable PbSRD5A–EGCG association after an initial ~30 ns adjustment period, with sustained NADPH-proximal contacts and a comparatively tighter binding-site pose than the parallel finasteride control. These convergent docking, MM-GBSA and MD results warrant future experimental assays to confirm competitive or non-competitive SRD5A inhibition by these compounds.

Advancement to knowledge:

SRD5A NADPH-cavity docking and MM-GBSA rescoring across nine chemically diverse AGA-relevant compounds - two prostaglandin analogues, a 4-azasteroid 5α-reductase inhibitor, two flavonoids, three small nutraceutical/hormonal compounds and an endogenous regulatory tetrapeptide - shows that structurally unrelated, non-classical SRD5A ligands can achieve MM-GBSA affinities comparable to or exceeding finasteride's at the same cofactor-proximal cavity. Latanoprost and dutasteride showed the most favourable predicted MM-GBSA binding energies, while EGCG was consistently strong across both scoring stages and was carried forward for MD validation. A 100 ns MD simulation of the PbSRD5A–EGCG complex reached a broadly stable equilibrium after an initial ~30 ns adjustment period, with sustained contact at several NADPH-proximal residues and a comparatively tighter binding-site pose than a parallel finasteride simulation, providing preliminary evidence for direct SRD5A modulation.

References:

[1] Sinclair R. *Exp Dermatol*. 2016 **25**:424 [PMID: 27061176]
[2] Bellani *D et al. Stem Cell Res Ther*. 2025 **16**:302 [PMID: 40518544]
[3] Hsing AW *et al Cancer Epidemiol Biomarkers Prev*. 2008 **17**:2525 [PMID: 18842992]
[4] Ntshingila S *et al JAAD Int.* 2023 **13**:150 [PMID: 37823040]
[5] Prabhakar MR *et al. Nat Prod Res*. 2021 **36**:5852. [PMID: 34937445]
[6] Timjan S *et al. ACS Omega.* 2025 **10**:58456. [PMID: 41502711]
[7] Mendoza-Lara DF *et al. Biointerface Res Appl Chem.* 2023 **13**:532. [DOI: 10.33263/BRIAC136.532]
[8] Han Y *et al. Nat Commun.* 2021 **12**:449 [PMID: 33469028]
[9] Miller WL & Auchus RJ. *Endocr Rev.* 2011 **32**:81 [PMID: 21051590]

[10] https://www.schrodinger.com/life-science/download/release-notes/release-2022-4/
[11] Genheden S & Ryde U. *Expert Opin Drug Discov.* 2015 **10**:449 [PMID: 25835573]
[12] Li J *et al. Proteins.* 2011 **79**:2794 [PMID: 21905107]
[13] Kim S *et al. Nucleic Acids Res*. 2023 **51**: D1373. [PMID:36305812]
[14] Friesner RA *et al. J Med Chem* 2004 **47**:1739 [PMID: 15027865]
[15] Halgren TA *et al. J Med Chem* 2004 **47**:1750 [PMID: 15027866]
[16] Barrón-Hernández YL & Tosti A. *Expert Opin Investig Drugs* 2017 **26**:515 [PMID: 28264599]
[17] Law S K. *Clin Ophthalmol* 2010 **4**:349 [PMID: 20463804]
[18] Kwon OS *et al. Phytomedicine* 2007 **14**:551 [PMID: 17092697]
[19] Hiipakka RA *et al. Biochem Pharmacol* 2002 **63**:1165 [PMID: 11931850]
[20] Blume-Peytavi U *et al. J Am Acad Dermatol*. 2012 **66**:794 [PMID: 21875758]
[21] Gubelin Harcha W *et al. J Am Acad Dermatol*. 2014 **70**:489 [PMID: 24411083]
[22] Ge F *et al. Fitoterapia*. 2018 **125**:258 [PMID: 29402482]
[23] Sudeep HV *et al. J Clin Cosmet Investig Dermatol*. 2023 **6**:3251 [PMID: 38021422]
[24] Fischer TW *et al. Br J Dermatol*. 2004 **150**:341 [PMID: 14996107]
[25] Fischer TW *et al. Br J Dermatol.* 2021 **184**:96 [PMID: 32271938]
[26] Hajem N *et al. Int J Cosmet Sci* 2013 **35**: 286 [PMID: 23488645]
[27] Shin JW & Huh CH. *Ann Dermatol*. 2025 **37**:327. [PMID: 41331712]
[28] Kearney CA *et al. Am J Clin Dermatol*. 2026 **27**:363 [PMID: 41714473]
[29] Sonthalia *et al. J Cosmo Trichol*. 2016 **2**:1 [DOI: 10.4172/2471-9323.1000105]

Caveat Emptor is applicable among the literate community where required and possible. The publisher, its journal, editors and the internal/external reviewers take adequate steps to check, evaluate, correct, edit, revise and improve content where possible and required.